Brown Carbon from Photooxidation of Glyoxal and SO_2 in Aqueous Aerosol

David O. De Haan,[1]* Lelia N. Hawkins,[2] Praveen D. Wickremasinghe,[1] Alyssa D. Andretta,[1] Juliette R. Dignum,[1] Audrey C. De Haan,[1] Hannah G. Welsh,[2] Elyse A. Pennington,[2] Tianqu Cui,[3,†] Jason D. Surratt,[3,4] Mathieu Cazaunau,[5] Edouard Pangui,[5] Jean-François Doussin[5]

1: Department of Chemistry and Biochemistry, University of San Diego, 5998 Alcala Park, San Diego CA 92117 USA

2: Department of Chemistry, Harvey Mudd College, 301 Platt Blvd, Claremont CA 91711 USA

3: Department of Environmental Sciences and Engineering, Gillings School of Global Public Health, University of North Carolina at Chapel Hill, Chapel Hill NC 27599 USA

4: Department of Chemistry, College of Arts and Sciences, University of North Carolina at Chapel Hill, Chapel Hill NC 27599 USA

5: Laboratoire Interuniversitaire des Systèmes Atmosphériques (LISA), UMR7583, CNRS, Université Paris-Est-Créteil (UPEC) et Université Paris Diderot (UPD), Institut Pierre Simon Laplace (IPSL), 94010 Créteil, France

†current address : Laboratory of Atmospheric Chemistry, Paul Scherrer Institute (PSI), 5232 Villigen-PSI, Switzerland

* Corresponding author: ddehaan@sandiego.edu, (619) 260-6882, (619) 260-2211 fax

ABSTRACT: Aqueous-phase dark reactions during the co-oxidation of glyoxal and S(IV) were recently identified as a potential source of brown carbon (BrC). Here, we explore the effects of sunlight and oxidants on aqueous solutions of glyoxal and S(IV), and on aqueous aerosol exposed to glyoxal and SO^2. We find that BrC is able to form in sunlit, bulk-phase, sulfite-containing solutions, albeit more slowly than in the dark. In more atmospherically relevant chamber experiments where suspended aqueous aerosol particles are exposed to gas-phase glyoxal and SO^2, the formation of detectable amounts of BrC requires an OH radical source and occurs most rapidly after a cloud event. From these observations we infer that this photobrowning is caused by radical-initiated reactions as evaporation concentrates aqueous-phase reactants and aerosol viscosity increases. Positive-mode electrospray ionization mass spectrometric analysis of aerosol-phase products reveals a large number of $C^xH^yO^z$ oligomers that are reduced rather than oxidized (relative to glyoxal), with the degree of reduction increasing in the presence of OH radicals. This again suggests a radical-initiated redox mechanism where photolytically-produced aqueous radical species trigger S(IV)-O^2 autooxidation chain reactions and, especially if aerosol-phase O^2 is depleted, glyoxal-S(IV) redox reactions. This process may contribute to daytime BrC production and aqueous-phase sulfur oxidation in the atmosphere. The BrC produced, however, is about an order of magnitude less light-absorbing than wood smoke BrC at 365 nm.

Keywords: photoreduction, oligomer, redox, sulfate formation, photosensitizer, photobrowning, photobleaching, viscosity

Introduction

Glyoxal and S(IV) react through aqueous-phase reactions to reversibly form the sulfonate adduct molecules glyoxal mono-bisulfite and glyoxal di-bisulfite (GDBS).[1] Sulfonate adducts are

resistant to oxidation by ozone and H^2O^2,[2] and are thus more stable than their precursor species. As a result, they are important reservoir species in the atmosphere, increasing the partitioning of both glyoxal and SO^2 to the aqueous phase.[3] Recently, it was shown that reactions in 1:1 mixtures of glyoxal and bisulfite ions (dissolved SO^2) in the presence of trace oxidants from the air can rapidly form oligomerized brown carbon (BrC) species, along with C^1 and C^3 sulfonate products, under slightly acidic conditions.[4] The C^1 sulfonate product, hydroxymethylsulfonate (HMS), has been detected at high concentrations in aerosol,[5-7] but was previously assumed to be formed only by the formaldehyde + S(IV) reaction. [7-9]

Secondary BrC formation in clouds and aqueous aerosol can potentially worsen climate change by absorbing solar radiation, a process known as the direct aerosol effect. The direct radiative forcing caused by the BrC component of aerosol has been estimated at 0.13 ±0.01 W m^{-2}.[10-13] In areas often impacted by biomass burning (e.g., the tropical mid and upper troposphere), BrC radiative forcing is greater than that of BC,[14] although generally it is less.[15, 16] All in all, BrC impacts are difficult to assess because its aging processes are not well understood.[17]

Many BrC mixtures have been shown via bulk aqueous experiments to be very susceptible to photobleaching[18-23] and oxidation by ozone,[24, 25] which has led to estimates of atmospheric BrC lifetimes that vary between ~30 min for BrC products derived from aldehyde + ammonium sulfate (AS) reactions[20, 26, 27] to several hours[18, 21, 28-31] to more than a day,[22, 25] depending on the BrC source and aging process. In contrast, recent studies where mixtures of amines, AS, and carbonyl species were irradiated in the aqueous aerosol phase reported photobrowning lasting a few hours.[32, 33] Other lab and field studies have observed initial browning of BrC mixtures, followed by bleaching after several hours of reaction time,[26, 28, 29, 31, 34] or even more complicated time-dependent changes.[35] This diversity in results from BrC aging studies indicates that there is no

reason to expect that BrC produced by different source reactions will behave similarly. Furthermore, the photobleaching and photobrowning behavior of glyoxal + S(IV) reactions has not been measured.

Here, we report measurements of the negative effects of sunlight on BrC formation in aqueous bulk mixtures of glyoxal and S(IV) at pH 5.5. In suspended aqueous aerosol particles exposed to glyoxal and SO^2 and undergoing cloud processing in a large chamber, we find that BrC formation is observed only in the presence of OH radical-initiated oxidation (using the photolysis of H_2O^2 as the OH radical source). Oligomerized aqueous-phase reaction products with unexpectedly low carbon oxidation states are explored via (+)-mode electrospray ionization mass spectrometry.

Methods

All solutions were made in 18 MΩ deionized water from solid reagents supplied by Sigma-Aldrich, unless otherwise specified. No unexpected or unusually high safety hazards were encountered.

Bulk aqueous experiments. To test the effects of sunlight on glyoxal + S(IV) mixtures, duplicate samples were created containing glyoxal (hydrolyzed from solid trimer by stirring in deionized water overnight, Fluka, > 99%), pH 5.5 acetate buffer, and sodium sulfite (Na^2SO^3, Spectrum) solution. This slightly acidic pH was selected because it is near the middle of the pH range observed for cloud droplets and sea spray aerosol.[36] Sample pairs in glass vials (with transmittance 50% cutoffs at ~350 nm) were placed in direct afternoon sunlight (late September, clear sky, 32°46' N, noon to 4 pm) in 4 h intervals, with sunlight blocked to one of each pair by aluminum foil, such that temperatures for sunlit and shaded samples remained within 2 ºC of each other, with shaded samples typically at the higher temperature. During each 4 h reaction interval, solar insolation

declined from ~1.0 to 0.8 kW/m^2. The UV/vis absorbance spectrum of each sample was measured in 1-cm pathlength quartz cuvettes after each 4 h reaction interval, and the sample was stored overnight at 4 ºC until the next sunny afternoon's solar irradiation interval. Precipitates formed upon cooling certain reaction samples were identified by powder X-ray diffraction (XRD, Bruker Apex II DUO) by comparison to authentic standards.

CESAM chamber experiments. To quantify the effects of simulated sunlight, OH radicals, and multiphase chemistry on glyoxal + S(IV) chemistry, aerosol seed particles were generated from 9 mM sodium sulfate (>99%) solution using an atomizer (TSI 3076) in experiments performed in the presence of SO^2 gas (Merck, > 99.95%). In experiments without SO^2 gas, particulate S(IV) was introduced by atomizing 9 mM sodium sulfite (Fluka, > 99%) solution. Since 9 mM Na^2SO^3 solutions are slightly basic (pH ~7.5), these solutions were buffered in most experiments to pH 5.5 using sulfuric acid. Gas-phase glyoxal was generated from a heated mixture of solid glyoxal trimer dihydrate and solid P^2O^5 (> 99%),[37] and introduced into the chamber in either a pulse (filling a glass bulb on a vacuum line to a well-determined pressure and flushing the contents into the chamber) or continuously (flowing dry N^2 through the solid mixture at ~140 °C into the chamber). Resulting glyoxal concentrations ranged from 150 to 640 ppb and were quantified by PTR-MS (KORE II) after calibration of signals by long-path in-situ FTIR using standard spectra.[38] During segments of certain experiments, hydrogen peroxide was added as an OH precursor by bubbling a 2 L/min flow of O^2 through a bubbler containing 30% HOOH (ACS-grade, non-stabilized) into the chamber.

CESAM is a pressure and temperature controlled stainless steel smog / cloud chamber with a fixed volume of 4.2 m^3 and three 6500 W Xe solar simulator lamps. Sampling flows are automatically compensated by additions of N^2 (evaporated from liquid) and high-purity O^2 at an

80:20 ratio. Gas phase contents were monitored by an SO^2 sensor, long-path FTIR (Bruker Tensor), PTR-MS, and sensors for temperature, RH, ozone, and NO^x. Dried aerosol properties, including total optical scattering/extinction and size distributions, were measured by cavity-attenuated phase shift / single-scattering albedo spectroscopy (CAPS-ssa, Aerodyne, 450 nm) and a scanning mobility particle sizer (SMPS, TSI 3080 / 3772), respectively. Aerosol and cloud droplet size distributions were also characterized by light scattering (PALAS welas Digital 2000, 0.4 to 15 μm range). At the end of each experiment, chamber-processed aerosol samples were collected on Teflon filters (1.0 μm pore size, 47 mm diam., Tisch Sci.) and frozen at -20 C until extraction and off-line ultra-high-performance liquid chromatography coupled with (+)-mode electrospray ionization high-resolution quadrupole time-of-flight mass spectrometry (UHPLC/ESI-HR-QTOFMS) analysis. Aerosol optical properties were also monitored without drying by PILS sampling into a waveguide UV/vis spectrometer with a 1 m pathlength and an inline total organic carbon (TOC) monitor. Gas phase signals were corrected for dilution from N^2 additions, and SMPS signals were corrected for dilution and wall losses. CAPS-ssa signals were corrected using 2^{nd}-order polynomial fits to daily calibrations with dried AS aerosol. Waveguide UV/vis data was normalized to TOC levels to generate mass absorption coefficients (MAC) in cm^2/gOC using the equation $MAC = 2.303A / bC$, where A is the measured $\log^{10}$ absorbance at a given wavelength, b is pathlength in cm, and C is the TOC level in g organic carbon cm^{-3}. The clean chamber was used for the waveguide reference spectrum. Due to temperature-dependent variations in detector response and lamp output, baselines often drifted to slightly negative absorbance values. During periods with measurable chromophores, the absorbance spectra appeared as expected. However, due to this drift, true MAC values may be slightly larger than our reported values.

All Teflon filter samples collected from chamber experiments were extracted with methanol (Optima LC/MS Grade, Fisher Scientific) by sonication for 45 min. The methanol extracts were dried under a gentle stream of high-purity nitrogen gas (Airgas) and reconstituted in 150 μL of 50:50 methanol and Milli-Q water. Filter extracts were analyzed by UHPLC/ESI-HR-QTOFMS operated in positive (+) ion mode, as previously described in detail.[39] Aliquots of 5 – 10 μL were injected onto a Waters ACQUITY UPLC HSS T3 column (2.1 × 100 mm, 1.8 μm particle size) and eluted at 0.3 mL min^{-1} with methanol and water solvent mixtures containing 0.1% ammonium acetate (LC-MS Chromasolv-grade, Sigma-Aldrich). Data were analyzed using Agilent MassHunter Version B.06.00 Build 6.0.633.0 qualitative software.

Results and Discussion

Bulk aqueous experiments. During solar irradiations, glyoxal / sulfite (HSO^{3-} at pH 5.5) samples had average temperatures of 35.5 and 37.5°C with and without exposure to direct sunlight, respectively. After four hours of exposure and overnight refrigeration, a white precipitate formed in glyoxal / HSO^{3-} samples, with higher quantities in samples that were shielded from solar radiation. This precipitate was identified as glyoxal di-bisulfate (GDBS) by comparing its powder XRD spectra with an authentic GDBS standard. GDBS is known to be formed reversibly in mixtures of glyoxal and sulfite, and is considered a reservoir species[1] in oxidant-free solution.[4]

Absorbance spectra of filtered 1:1 glyoxal:HSO^{3-} mixtures are shown in Figure 1. Modest absorbance in the actinic range was observed initially upon sample mixing, along with an absorbance maximum at 292 nm observed in an earlier study.[4] After 4 h of sunlight exposure, absorbance was saturated below 330 nm and enhanced by factors of 2.0 to 3.4 out to 480 nm. (Absorbance was below detection limits beyond 480 nm.) In duplicate temperature-matched

samples shielded from sunlight, the absorbance was enhanced by factors between 3.3 and 5.5 over the same wavelength range, a change which is much larger than run-to-run variation (~15%). The enhancement in absorbance in the dark was larger than in sunlight at all wavelengths between 330 and 480 nm, with an average dark / sunlight enhancement ratio of 1.6 ±0.2. These results demonstrate that photobleaching of BrC products formed by glyoxal + sulfite reactions is occurring, but this photobleaching cannot keep pace with BrC production in these sunlit (250 mM) solutions where no OH precursor was added.

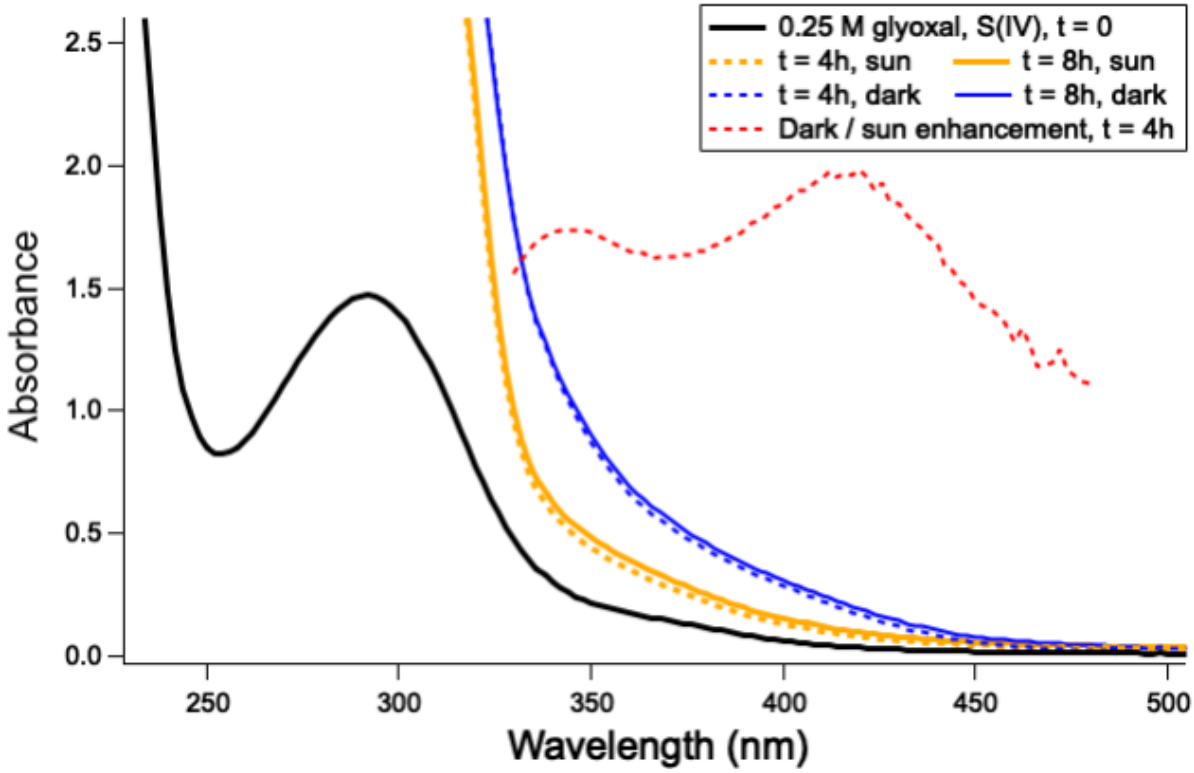

Figure 1: Absorption spectrum of filtered pH 5.5 reaction mixture containing 0.25 M Glyoxal and 0.25 M HSO_3^- before (black line) and after one and two 4 h periods of solar irradiance (gold) or dark processing at similar temperatures (blue). 4 h reaction time (dashed lines); 8 h reaction time (solid colored lines). The ratio of dark vs sun absorption enhancement (dashed red line) is shown for wavelengths beyond 320 nm; the average ratio between 330 and 480 is 1.6 ±0.2.

CESAM chamber experiments with gas-phase glyoxal and SO_2. Glyoxal + S(IV) experiments conducted in the CESAM chamber are summarized in Table 1. Glyoxal concentrations (150 to 640 ppb) were chosen to match an earlier study of glyoxal + S(IV) dark chemistry. In Experiments 1-4, 140 to 600 ppb SO^2 gas was added to the chamber, and dried seed aerosol particles were generated from Na^2SO^4 solutions. The SO^2 concentration range was chosen to simulate an extremely polluted atmosphere (bracketing China's 1-hour "grade II" air quality standard for SO^2 of 500 ppb), and to approach the predicted SO^2 gas-phase concentration if gas-aqueous equilibrium were reached in Experiments 5-7 (670 ppb), where dried seed aerosol particles were produced from Na^2SO^3 solution as the S(IV) source. The sulfite solution was buffered to pH 5.5 with sulfuric acid in Experiments 6 and 7, resulting in aerosol initially consisting of mixed, effloresced $NaHSO^3$ and $NaHSO^4$. The pH of the unbuffered Na^2SO^3 solution used to generate seed aerosol particles in Experiment 5 was ~7.5.

In Experiment 1 (Figure 2), gas-phase glyoxal and SO^2 were added to the chamber containing deliquesced sodium sulfate aerosol at RH > 90%. Glyoxal was added continuously after 14:03 (local time), while SO^2 was added in a single pulse at 14:44. Neither of these additions caused a significant increase in dried particle mass or browning, although TOC rose gradually by 10% starting after the SO^2 addition, likely due to some aqueous-phase glyoxal-SO^2 adduct formation.

Table 1: CESAM Chamber Cloud Processing Experiments with S(IV) and Gas-Phase Glyoxal

Expt.	Figure	$[GX]_g$ (ppb)[a]	Seed Aerosol Types[b]	$[SO_2]_g$ (ppb)	$[HOOH]_g$ added	Secondary aerosol produced[c] ($\mu g/m^3$)	MAC max (cm^2/gOC) 365 nm	Min. albedo reached, 450 nm	Δ albedo (final cloud)
1	Fig. 2	170 ±10	Na_2SO_4	140 ±5	Yes, cloud 3	57 ±4	100 ±40 (no data after cloud 3)	0.75 ±0.02	-0.15 ±0.03
2	Fig S3	170 then 310	Na_2SO_4	550	Yes, pre-cloud only	40	380	0.83	-0.03
3	Fig S4	640	Na_2SO_4[d]	520	No	26	120	0.86	-0.012
4	Fig. 3	150	Na_2SO_4[d]	600	Yes, cloud 2	65	1800	0.89	-0.06
5	Fig S2	170	$Na_2\mathbf{SO_3}$	8 ±1[e]	Yes, cloud 3	20	2000	0.92	noisy
6	Fig S1	150	pH 5.5 $Na_2\mathbf{SO_3}$	10 ±1[e]	No	6	2600	0.88	noisy
7	Fig. S7	490	pH 5.5 $Na_2\mathbf{SO_3}$ in N_2	20 ±1[e]	No	6	1200	0.85	-0.02 w/ RH

Notes: All runs had 2-3 cloud events, with solar simulator lights turned on for the last cloud event (except in Experiment 2, where lights were on under dry conditions only, followed by 2 dark cloud events). Uncertainties listed for Experiment 1 are typical for all experiments unless otherwise stated. **a**: based on PTR-MS signals at *m/z* 31 and on pressure in glass transfer bulb in Experiment 1, calibrated by long-path FTIR. **b**: diffusion dried and suspended in high-purity air unless otherwise stated. **c**: measured by SMPS, assuming aerosol density of 1.0. **d**: flash-dried (liquid particles sent into dry chamber). **e**: Equilibrated from sulfite seed particles, concentration given is that measured after seed particle addition was complete. Higher levels were briefly observed upon humidification, see corresponding figures.

Normally, chamber cloud events cause a decrease in dried particle mass that is measurable by SMPS, due to wet deposition of some cloud droplets containing the aerosol particles that served as cloud condensation nuclei. (The lifetime of a 200 nm diameter particle in the chamber is on the order of a day, but when activated into a 5 μm cloud droplet, its lifetime shortens to several minutes.) An example of this wet deposition can be seen in the 18% dried particle mass loss after cloud 1 at 13:33, or 8 to 15% mass losses after the clouds in Figures S1 and S2. In contrast, once

glyoxal and SO^2 gases were present in the chamber, a water vapor addition at 15:15 and cloud 2 caused respective increases in particle mass of 22 and 12%. The fact that TOC signals do not also increase in a correlated manner with SMPS mass indicates that this increase in particle mass is mainly due to sulfite or sulfate formation. Since the Henry's law coefficient of SO^2 is only 1.47 M/atm, dissolved SO^2 (or H^2SO^3) concentrations are expected to remain below 1 μM, unless a base is present to react with H^2SO^3 to produce HSO^{3-} or $SO^{3\,2-}$ ions. Indeed, negligible aerosol-phase sulfur was observed in an earlier study where wet NaCl aerosol was exposed to $SO^2(g)$.[4] A proton transfer reaction involving sulfate ions is thus likely responsible for the dark growth in aerosol dry mass observed in Experiment 1:

$$SO^2(g) + H^2O(l) \leftrightharpoons H^2SO^3(aq)$$

$$SO^{4\,2-}(aq) + H^2SO^3(aq) \rightarrow HSO_3^-(aq) + HSO_4^-(aq)$$

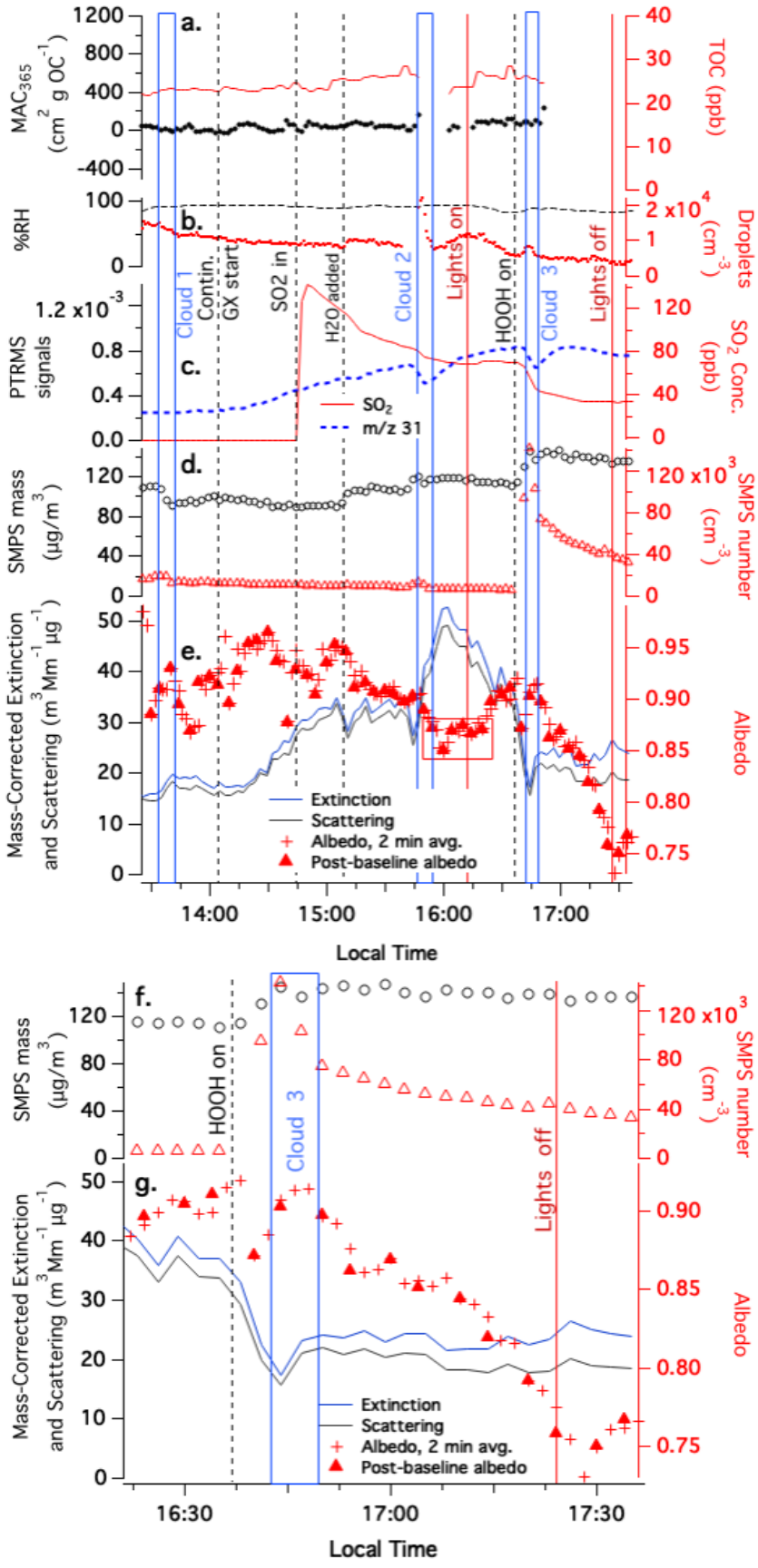
a.
b.
c.
d.
e.
f.
g.
MAC365 (cm2 g OC-1)
TOC (ppb)
%RH
Droplets (cm-3)
PTRMS signals
SO2 Conc. (ppb)
SO2
m/z 31
SMPS mass (µg/m3)
SMPS number (cm-3)
Mass-Corrected Extinction and Scattering (m3 Mm-1 µg-1)
Albedo
Extinction
Scattering
Albedo, 2 min avg.
Post-baseline albedo
Cloud 1
Contin. GX start
SO2 in
H2O added
Cloud 2
Lights on
HOOH on
Cloud 3
Lights off
14:00
15:00
16:00
17:00
16:30
17:30
Local Time

Figure 2: Gas-phase glyoxal and SO^2 uptake during Experiment 1 with deliquesced Na^2SO^4 aerosol in CESAM chamber, 9:50 start time. Three cloud events, start of continuous glyoxal addition, SO^2 addition, start and end of chamber illumination, and start of HOOH addition are labeled. Panel **a**: total organic carbon readings and mass absorption coefficients at 365 nm from PILS/waveguide UV-vis, (re-zeroed at 16:03), color coded to axes. **b**: chamber RH and droplet spectrometer counts, color coded to axes. **c**: water- and dilution-corrected PTR-MS data (*m/z* 31 glyoxal fragment, blue dotted line); and SO^2 concentrations in ppb from dedicated sensor (red line). **d**: SMPS total mass (assuming density = 1 g/cm^3) and counts shown next, color-coded to axes. **e**: CAPS-ssa data at 450 nm (mass-corrected extinction, blue line; mass-corrected scattering black line; single-scattering albedo, red dots; ssa measured immediately after gas-phase baseline, red triangles; red box indicates points measured beyond calibration range of instrument). **f** and **g**: Copies of panels **d** and **e**, zoomed in on end of experiment to better show onset times of nucleation event and browning.

After the chamber solar simulator lights were turned on, HOOH(g) was added to the chamber as an OH radical source, about a minute before cloud event 3. As soon as HOOH was added, particle counts increased more than 10-fold and particle mass increased by 27% due to a nucleation event, likely caused by oxidation of SO^2 by HOOH. (The identity of the oxidant as HOOH and not OH radicals is supported by Experiment 2 (Figure S3), where new particle nucleation is seen *in the dark* when SO^2 (g) and HOOH(g) are present and RH reaches 25%.) During cloud event 3, glyoxal (g) concentrations temporarily fell from 120 to 90 ppb while SO^2 (g) concentrations fell from 71 to 43 ppb. While the temporary loss of glyoxal was similar to that observed during the previous (HOOH-free and dark) cloud event 2, the drop in SO^2 (g) concentrations during cloud 3 was several

times larger than during cloud 2, indicating the importance of SO^2 + HOOH reactions in driving SO^2 uptake to the aqueous phase.

No detectable BrC formed during the dark portion of Experiment 1: no rise in MAC at 365 nm or convincing drop in albedo at 450 nm was observed. As cloud 3 dissipated, however, the single-scattering albedo measured at 450 nm began to decline from 0.90 to 0.75, stopping only when the lights were turned off 40 minutes later. Therefore, this photobrowning was driven by either direct photolysis or by OH radical reactions, and occurred most rapidly after the evaporation of cloud droplets. Furthermore, it appears that neither cloud events nor photolysis / OH radical-initiated photooxidation are sufficient to cause uptake and rapid photobrowning by glyoxal and SO^2 in aqueous aerosol particles; rather, both are required.

Similar experiments on BrC formation from SO^2 (g) and GX (g) uptake onto Na^2SO^4 seeds, but with (Experiment 4) and without HOOH addition (Experiment 3) during the final cloud event, are compared in Figure 3. In both experiments, cloud 1 occurred in the dark without HOOH, and did not produce SOA mass or BrC, as before. Albedo at 450 nm declined by less than 0.012, and the MAC at 365 nm increased by less than 80 $cm^2\ g^{-1}$, both within the noise of these data sets. In Experiment 3, cloud 2 occurred with the lights on but in the absence of HOOH. Under these conditions, no BrC, and less than 5 $\mu g/m^3$ of aerosol, was produced (Figure S4). In contrast, in Experiment 4 with lights and HOOH, cloud 2 produced 65 $\mu g/m^3$ of secondary aerosol and substantial BrC, visible from the large increase in MAC and large decrease in albedo in Figure 3. As before, a drop in albedo at 450 nm and an increase in MAC at 365 nm occur once light, HOOH, and a cloud event are all present, suggesting that aqueous photobrowning reactions involving OH radicals are responsible for BrC production. (The very small MAC increase at 365 nm before

cloud 2 is likely due to limited photobrowning involving lower levels of radical generation by direct photolysis or photosensitization.)

CESAM chamber experiments with sulfite aerosol. In a previous study, BrC production was observed when gas-phase glyoxal interacted with aqueous sulfite-containing aerosol particles in a flowing system with a 1-minute residence time, without the need for OH radical sources or sunlight.[4] Experiments 5 – 7 (Figures S1, S2, S5, and S6) explore this system to try to better understand differences between experiments where S(IV) is initially supplied in the gas or aerosol phase. In all three experiments, dried sulfite-containing aerosol were added to the dry chamber, accompanied by relatively small amounts (8-20 ppb) of gas-phase SO^2, likely released from the aqueous phase during initial aerosol generation (before drying). The addition of glyoxal gas under dry conditions (RH < 5%) did not increase SMPS mass or MAC at 365 nm. This is consistent with previous flow chamber experiments with sulfite-containing aerosol, where glyoxal did not cause aerosol browning or substantial growth under dry conditions.[4]

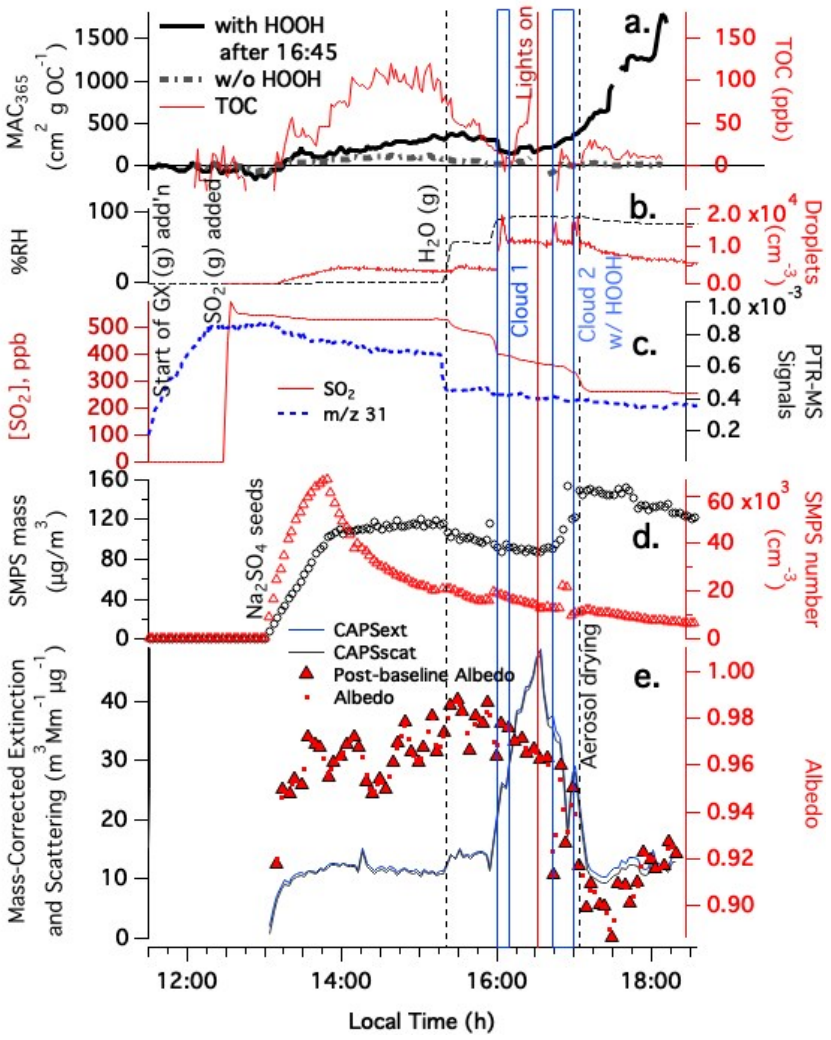

Figure 3: Gas-phase glyoxal and SO^2 uptake Experiment 4 with Na^2SO^4 aerosol in the CESAM chamber, 8:31 start time. Glyoxal gas added continuously after 11:30. SO^2 addition, water vapor addition, two cloud events, start of chamber illumination by solar simulator lights, and the onset of aerosol drying on the way to SMPS and CAPS-ssa instruments are labeled. Panel **a**: mass absorption coefficients measured by PILS – waveguide - TOC at 365 nm in Expt. 4 with HOOH during cloud 2 (red line) compared with Expt. 3 (no HOOH added, gray dash-dot line, complete data in Figure S4). **b**: chamber RH and droplet spectrometer counts, color-coded to axes. **c**: water- and dilution-corrected PTR-MS data from chamber (*m/z* 31 glyoxal fragment, blue dotted line) and SO^2 concentrations in ppb from dedicated sensor (red line). **d**: SMPS total mass (assuming density = 1 g/cm^3) and counts, color-coded to axes. **e**: CAPS-ssa data at 450 nm (mass-corrected extinction, blue line; mass-corrected scattering, black line; 2-min averaged single-scattering albedo, red dots, and albedo measured immediately after instrument baselines, red triangles).

In Experiments 5-7, once the chamber was humidified, most glyoxal gas was immediately lost from the gas phase, and TOC levels increased, showing that glyoxal was taken up by the deliquesced, sulfite-containing aerosol particles. At the same time, SO^2 gas was released from the aerosol to the gas phase as equilibrium with aqueous-phase sulfite was established. However, most of the SO^2 gas released upon aerosol deliquescence was recaptured within 15 minutes, presumably due to aqueous reactions with glyoxal occurring in aerosol particles and on chamber walls. In Experiment 5, SO^2 recapture resulted in net growth of the aerosol, while in experiments where the aerosol was acidified to pH 5.5 (Experiments 6 and 7), no net growth was observed. In all three experiments, a large increase in MAC was observed upon SO^2 recapture under dark conditions, consistent with the dark production of BrC previously observed for this system.[4] These observations are strong evidence that glyoxal can form light-absorbing BrC in dark reactions with high concentrations of bisulfite ions in deliquesced, mildly acidic aerosol, but not under dry conditions.

Since aerosol deliquescence is enough to cause glyoxal uptake and browning with Na^2SO^3 or $NaHSO^3$ aerosol, even in the dark and without HOOH, it appears that the mechanism of BrC formation is different when starting with gas-phase SO^2 as compared to aerosol-phase sulfite. In bulk solution, or when deliquesced, sulfite-containing aerosol is exposed to gas-phase glyoxal, glyoxal-sulfite adduct molecules evidently reach such high concentrations in the aqueous phase that BrC can form in the dark, as observed in both types of experiments. However, when gas-phase SO^2 is the S(IV) source, glyoxal-sulfite adduct molecules produced after uptake of both SO^2 and glyoxal to the aqueous phase are likely present at much lower concentrations. Under these conditions, which are more relevant to the atmosphere, the formation of detectable amounts of BrC oligomers requires an OH radical source and occurs most rapidly after a cloud event.

Mass spectral analysis of chamber-processed aerosol. The molecular formulas of compounds detected by UHPLC/(+)ESI-HR-QTOFMS in filter extracts from Experiments 1 and 3-7 are summarized in Figures 4 and S7 as well as in Table S1. The molecules detected in the aerosol phase depended most strongly on the oxidant present in the chamber, rather than on the source of S(IV). In Experiment 7, performed without oxidants (the aerosol was suspended in N^2 containing no more than a few ppm O_2, and no HOOH was added at any point), a much higher fraction of detected organic aerosol molecules fell within the O/C ratio range expected for glyoxal oligomers, shown in Figure 4 as the region between the two red lines. These oligomers include C^7 – C^{14} species, which we note are larger than the C^4 dimers and C^6 trimers commonly detected in aqueous GX mixtures. These larger particulate-phase oligomers likely formed during the evaporative stage of cloud processing.

The ion-count-weighted average parameters of molecules detected by UHPLC/(+)ESI-HR-QTOFMS in each experiment are summarized as a function of oxidant used in Table 2. In the absence of O^2 and HOOH but with sunlight, the average oxidation state of carbon in detected product molecules was -0.43, significantly lower than carbon's +1.0 oxidation state in glyoxal and its oligomers. This suggests that significant aerosol-phase redox reactions have taken place, with S(IV) species presumably serving as reducing agents. Since glyoxal and S(IV) are known to form stable adduct molecules through aqueous phase reactions when oxidants are excluded,[1] the aerosol redox reactivity we observed may be triggered by radical species formed by direct photolysis of BrC species or by photosensitization. These radicals could initiate direct redox chemistry between S(IV) and glyoxal, allowing the formation of reduced organic species along with sulfate ions.

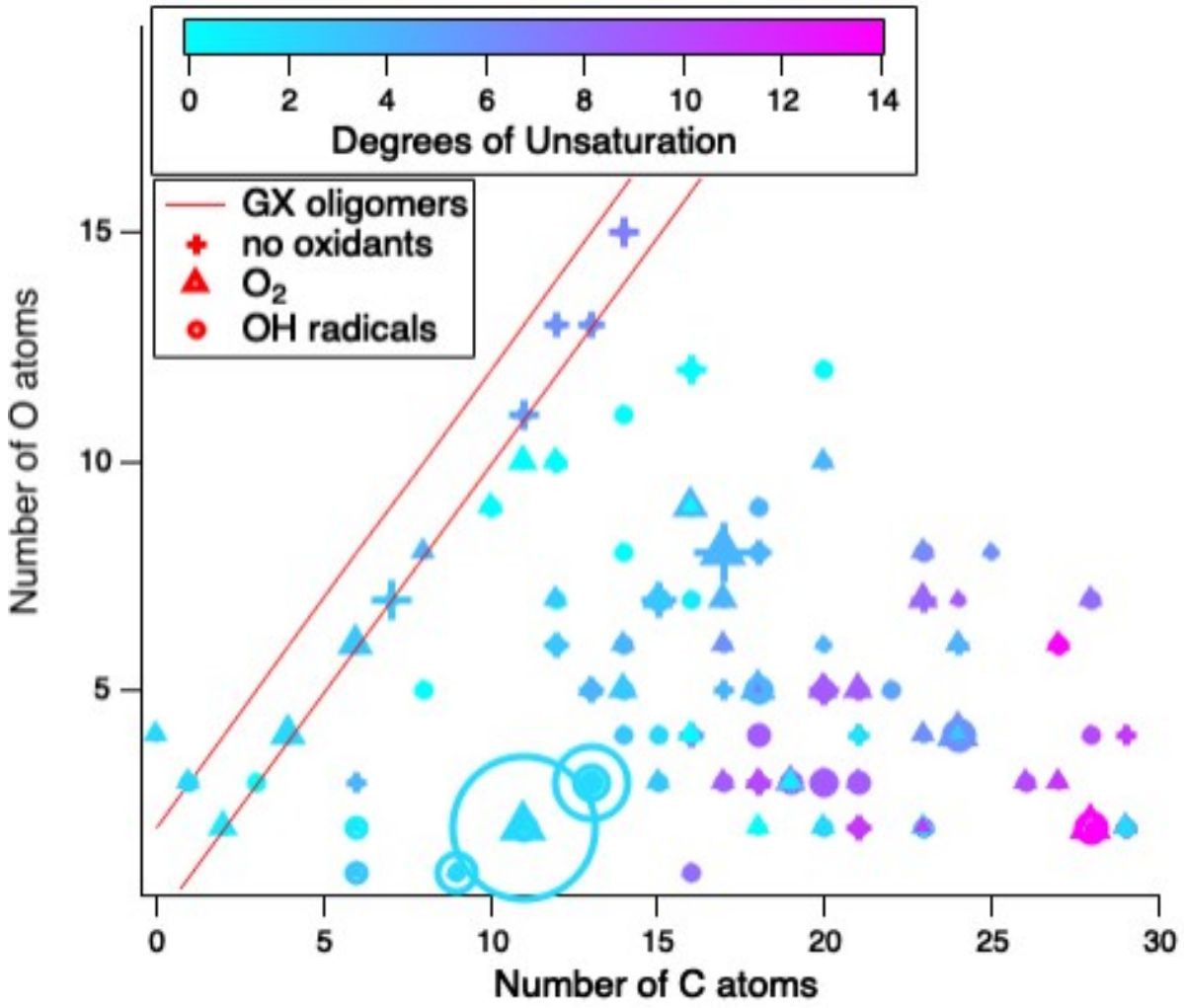

Figure 4: Summary of molecular formula detected by UHPLC/(+)ESI-HR-QTOFMS analysis of filter extracts of chamber aerosol in Experiments 1 and 3-7, graphed in terms of numbers of O and C atoms. Symbols indicate oxidant present: no oxidant (+), and O^2 (triangles), or OH radicals (circles). Colors indicate degrees of unsaturation, symbol areas are proportional to average peak areas across experiments with the given oxidant, and red lines indicate expected range of particulate glyoxal oligomers. Multiple symbols of the same shape and color centered on one location represent isomers with identical mass but distinguished by retention times.

Table 2: Average Parameters of Molecules Detected by UHPLC/(+)ESI-HR-QTOFMS in Aerosol Particles as a Function of Oxidant Used in Glyoxal + S(IV) + Sunlight -Experiments

Average Parameter	No oxidant	O_2		OH radical		
Experiment number	7	3	6	1	4	5
Degrees of unsaturation	5.0	5.4	4.8	6.0	3.2	5.8
		x = 5.1 ±0.4		x = 4.0 ±1.6		
O/C ratio	0.52	0.42	0.40	0.39	0.24	0.34
		x = 0.41 ±0.01		x = 0.28 ±0.08		
C atoms / molecule	16.5	17.0	16.6	17.9	13.7	18.2
		x = 16.8 ±0.3		x = 15.1 ±2.5		
C oxidation state	-0.45	-0.68	-0.79	-0.72	-1.24	-0.79
		x = -0.73 ±0.07		x = -1.09 ±0.3		

Notes: Average values for each experiment are weighted by MS ion counts for each detected species. Averages (with uncertainties) calculated from multiple experiments are shown as x values.

In Experiments 3 and 6, performed in N^2 / O^2 mixtures instead of only N^2 gas, average carbon oxidation state and average O/C ratio in detected products both declined further. In the presence of O^2, S(IV) autooxidation is known to be initiated by radical species or transition metals, and this autooxidation involves a catalytic chain reaction where sulfoxy radicals are intermediates.[40] In our experiments, any contribution to S(IV) autooxidation from trace metal contaminants is likely suppressed by glyoxal,[41] so we can assume that photolytically-produced radical species or BrC photosensitization starts the S(IV) autooxidation chain reaction. Sulfoxy radicals, like OH radicals, can react with organic species by abstracting hydrogen atoms[42] or adding to C=C double bonds.[43] Addition of sulfoxy radicals to C=C double bonds would generate organosulfate species, which do not ionize well in (+)-mode ESI due to their negative charge.[44] Indeed, only 3 out of the 126 aqueous aerosol species detected by (+)-mode ESI-MS contained sulfur in our experiments, indicating that only the H-abstraction reaction pathway is being probed here. Since organic species with more double bonds have fewer hydrogens, higher carbon oxidation states,

and are more susceptible to radical addition than species with fewer double bonds, our use of (+)-mode electrospray ionization likely exhibits a detection bias towards more reduced products. However, the similar values for average degree of unsaturation across all types of experiments, with their different radical levels, suggests that this bias is rather small. Indeed, Walser *et al.*[45] compared positive and negative mode ESI-MS analysis of SOA produced by limonene ozonolysis and found that the (+)-mode ESI bias in the measured average O/C was only -0.07 (O/C = 0.43 in (+)-mode vs. 0.50 in (-)-mode, both significantly higher than O/C = 0 in the reactant limonene). In the current work the O/C ratio difference between the reactants (glyoxal and its oligomers with O/C ≥ 1) and the products detected by (+)-mode ESI are 7 to 10× larger than this detection bias.

In the presence of dissolved O^2 neither hydrogen abstraction nor radical addition would be expected to form products with lower O/C ratios than the reactants, since O^2 normally adds to organic radical species produced by either pathway. Thus, the additional decline in both carbon oxidation state and O/C ratios in experiments where O^2 was present suggests that aerosol-phase O^2 is depleted by the time oligomers form. In other words, after launching the aqueous-phase autooxidation of S(IV) and the production of sulfoxy radicals, resulting in greater production of organic radicals, O^2 may become depleted in evaporating aqueous aerosol due to molecular crowding (increased sinks) and increased viscosity, which slows O^2 diffusion into the particles. If aerosol-phase O^2 is depleted, organic radicals can react more readily with other nearby organic species, producing oligomers with lower O/C ratios, as observed. O^2 depletion in aerosol particles, or the related change in photochemical products to photoreduction and oligomerization, has been observed in recent studies of viscous aerosol phases.[23, 46] Additionally, aqueous aerosol containing glyoxal have been documented to become highly viscous.[47] We hypothesize that evaporation of

cloud droplets in the atmosphere can create similarly viscous aerosol particles, which then have the potential to become depleted in O^2.

With the addition of HOOH as an OH radical precursor, measured average O/C ratios and carbon oxidation states of aerosol phase organic species drop even further than that caused by the addition of O^2. This result, while again counter-intuitive, is the same trend as before. Positive-mode ESI-MS also has a detection bias against organic acids, which are the products of OH radical addition in the presence of dissolved O^2, but this detection bias is again unlikely to explain simultaneous declines in O/C ratios and carbon oxidation states in the presence of OH radicals. Instead, the declines are likely due to higher initial radical concentrations triggering more S(IV) autooxidation chain reactions, resulting in more sulfoxy radicals producing greater numbers of organic radical species, which more quickly deplete aqueous-phase O^2 and then form less-oxygenated oligomers. We note, however, that the average number of carbon atoms per detected molecule does not change significantly under the different oxidant conditions. This suggests that different oxidant conditions are changing the type of oligomers formed in the glyoxal + S(IV) system (more oxidized or more reduced), rather than causing large changes in the quantity or total extent of oligomerization.

Finally, we note that in experiments where OH radicals were present, the average degree of unsaturation in detected organic aerosol species does not change significantly from other experiments. Since the formation of BrC species requires the production of molecules with delocalized π bonds in order to absorb visible light,[17, 48] one might expect the average degree of unsaturation to increase in this system, where BrC was formed. Instead, these results indicate that the majority of the detected organic aerosol species are not light-absorbing BrC molecules. Instead, a small minority of highly-absorbing species are apparently responsible for the optical

properties of BrC aerosol formed by reactions between S(IV) and glyoxal, as has been observed in other reaction systems that form BrC.[49]

Atmospheric Significance. These laboratory experiments show that gas-phase glyoxal and SO^2 can be taken up by cloud droplets and, in the presence of an OH radical source, will form sulfate and reduced (rather than oxidized) oligomerized species including BrC. From these observations we infer that radical-initiated redox reactions between SO^2 and glyoxal have taken place in O^2-depleted, post-cloud aqueous aerosol particles. The role of glyoxal in these reactions is likely two-fold. First, like any small aldehyde, glyoxal reacts with dissolved SO^2 to form sulfonate adducts,[1, 3, 8, 50, 51] which keep the two reactant species in physical proximity and, we hypothesize, make subsequent redox reactions between them more likely. Second, glyoxal oligomerization increases the viscosity of aqueous aerosol,[47, 52] making O^2 depletion more likely. These roles suggest that other combinations of (1) small, water-soluble, sulfonate-adduct-forming aldehydes, plus (2) oligomer-forming organic molecules might also be able to generate the conditions necessary for radical-initiated SO^2 – aldehyde redox reactions and BrC oligomer production in the aqueous aerosol phase.

While the concentrations of glyoxal (> 150 ppb) and SO^2 (> 140 ppb) used in these studies were very high, the total aldehyde concentration in Beijing can approach ~100 ppb,[53] and SO^2 concentrations as high as 50 ppb were measured in 2010 in the lower planetary boundary layer over eastern China.[54] Furthermore, estimates of global aerosol phase have shown that most aerosol particles are semi-solids, especially in the middle and upper troposphere.[55] Thus, it may be possible that SO^2 can engage in redox reactions with small aldehyde molecules in semi-solid aerosol particles in many regions of the troposphere.

The BrC MAC^{365} levels of 0.12 – 0.26 m^2 gOC^{-1} (or 1200 – 2600 cm^2 gOC^{-1}) measured in experiments 4 - 7 compare with BrC MAC^{365} mean levels of 0.8 – 2.4 m^2 gOC^{-1} recently measured in Asian cities[56, 57] and with 0.5 - 5 m^2 gOC^{-1} BrC MAC^{365} measured in wood smoke.[58, 59] The secondary BrC produced by glyoxal + SO^2 reactions in this work therefore appears to be approximately an order of magnitude less absorbing than BrC from wood smoke.

Acknowledgments: This work was funded by NSF grants AGS-1523178, AGS-1826593, and AGS-2218491. L. N. Hawkins was funded by the Barbara Stokes Dewey Foundation and Research Corporation (CCSA 22473). CNRS-INSU is gratefully acknowledged for supporting CESAM as an open facility through the National Instrument label. This project/work has received funding from the European Union's Horizon 2020 research and innovation programme through the EUROCHAMP-2020 Infrastructure Activity under grant agreement No 730997. UNC acknowledges the National Institute of Environmental Health Sciences (NIEHS) grant No. P30ES010126 for the UHPLC/ESI-HR-QTOFMS instrument used during this study. We thank Bénédicte Picquet-Varrault for posting the chamber dataset.

Data availability: Concentration-time profiles for the large chamber experiments are freely accessible in .edf format through the chamber database at data.eurochamp.org maintained by AERIS for the benefit of ACTRIS ERIC. (Expt. 1: https://doi.org/10.25326/4HS3-M215. Expt 2: https://doi.org/10.25326/XE7Z-EC10. Expt. 3: https://doi.org/10.25326/5X59-Q090. Expt. 4: https://doi.org/10.25326/D3DD-Y688. Expt 5: https://doi.org/10.25326/J1ZN-X623. Expt 6: https://doi.org/10.25326/R7T9-8X80. Expt 7: https://doi.org/10.25326/4841-QM92.)

Supporting information

A list of aerosol-phase compounds detected in each experiment by UHPLC/ESI-HR-QTOFMS, summary plots for chamber experiments 2, 3, and 5 – 7, a sample of time-dependent UV-vis spectra in experiment 7 from water-soluble aerosol particles collected by PILS, and a graph summarizing the O/C ratio, H/C ratio, and degree of unsaturation of detected aerosol-phase compounds.

References Cited

1. Olson, T. M.; Hoffmann, M. R., Kinetics, mechanism, and thermodynamics of glyoxal-S(IV) adduct formation. *J. Phys. Chem. A* **1988,** *92*, (2), 533-540. doi:10.1021/J100313A056
2. Zuo, Y., Light-induced oxidation of bisulfite-aldehyde adducts in real fog water. *Naturwissenschaften* **1994,** *81*, (11), 505-507. doi:10.1007/BF01132683
3. Olson, T. M.; Hoffmann, M. R., Hydroxyalkylsulfonate formation: its role as a S(IV) reservoir in atmospheric water droplets. *Atmos. Environ.* **1989,** *23*, (5), 985-997. doi:10.1016/0004-6981(89)90302-8
4. De Haan, D. O.; Jansen, K.; Rynaski, A. D.; Sueme, W. R. P.; Torkelson, A. K.; Czer, E. T.; Kim, A. K.; Rafla, M. A.; De Haan, A. C.; Tolbert, M. A., Brown Carbon Production by Aqueous-Phase Interactions of Glyoxal and SO2. *Environ. Sci. Technol.* **2020,** *54*, (8), 4781-4789. doi:10.1021/acs.est.9b07852
5. Song, S.; Gao, M.; Xu, W.; Sun, Y.; Worsnop, D. R.; Jayne, J. T.; Zhang, Y.; Zhu, L.; Li, M.; Zhou, Z.; Cheng, C.; Lv, Y.; Wang, Y.; Peng, W.; Xu, X.; Lin, N.; Wang, Y.; Wang, S.; Munger, J. W.; Jacob, D. J.; McElroy, M. B., Possible heterogeneous chemistry of hydroxymethanesulfonate (HMS) in northern China winter haze. *Atmos. Chem. Phys.* **2019,** *19*, (2), 1357-1371. doi:10.5194/acp-19-1357-2019
6. Chen, C.; Zhang, Z.; Wei, L.; Qiu, Y.; Xu, W.; Song, S.; Sun, J.; Li, Z.; Chen, Y.; Ma, N.; Xu, W.; Pan, X.; Fu, P.; Sun, Y., The importance of hydroxymethanesulfonate (HMS) in winter haze episodes in North China Plain. *Environ. Res.* **2022,** *211*, 113093. doi:https://doi.org/10.1016/j.envres.2022.113093
7. Liu, J.; Gunsch, M. J.; Moffett, C. E.; Xu, L.; El Asmar, R.; Zhang, Q.; Watson, T. B.; Allen, H. M.; Crounse, J. D.; St. Clair, J.; Kim, M.; Wennberg, P. O.; Weber, R. J.; Sheesley, R. J.; Pratt, K. A., Hydroxymethanesulfonate (HMS) Formation during Summertime Fog in an Arctic Oil Field. *Environ. Sci. Technol. Lett.* **2021,** *8*, (7), 511-518. doi:10.1021/acs.estlett.1c00357
8. Olson, T. M.; Hoffmann, M. R., On the kinetics of formaldehyde-S(IV) adduct formation in slightly acidic solution. *Atmos. Environ. (1967)* **1986,** *20*, (11), 2277-2278. doi:https://doi.org/10.1016/0004-6981(86)90318-5
9. Rao, X.; Collett, J. L. J., Behavior of S(IV) and formaldehyde in a chemically heterogeneous cloud. *Environ. Sci. Technol.* **1995,** *29*, (4), 1023-1031. doi:10.1021/es00004a024

10. Brown, H.; Liu, X.; Feng, Y.; Jiang, Y.; Wu, M.; Lu, Z.; Wu, C.; Murphy, S.; Pokhrel, R., Radiative effect and climate impacts of brown carbon with the Community Atmosphere Model (CAM5). *Atmos. Chem. Phys.* **2018,** *18*, (24), 17745-17768. doi:10.5194/acp-18-17745-2018
11. Wang, X.; Heald, C. L.; Liu, J.; Weber, R. J.; Campuzano-Jost, P.; Jimenez, J. L.; Schwarz, J. P.; Perring, A. E., Exploring the observational constraints on the simulation of brown carbon. *Atmos. Chem. Phys.* **2018,** *18*, (2), 635-653. doi:10.5194/acp-18-635-2018
12. Saleh, R.; Marks, M.; Heo, J.; Adams, P. J.; Donahue, N. M.; Robinson, A. L., Contribution of brown carbon and lensing to the direct radiative effect of carbonaceous aerosols from biomass and biofuel burning emissions. *J. Geophys. Res. Atmos.* **2015,** *120*, (19), 10,285-10,296. doi:10.1002/2015JD023697
13. Feng, Y.; Ramanathan, V.; Kotamarthi, V. R., Brown carbon: a significant atmospheric absorber of solar radiation? *Atmos. Chem. Phys.* **2013,** *13*, (17), 8607-8621. doi:10.5194/acp-13-8607-2013
14. Zhang, A.; Wang, Y.; Zhang, Y.; Weber, R. J.; Song, Y.; Ke, Z.; Zou, Y., Modeling the global radiative effect of brown carbon: a potentially larger heating source in the tropical free troposphere than black carbon. *Atmos. Chem. Phys.* **2020,** *20*, (4), 1901-1920. doi:10.5194/acp-20-1901-2020
15. Andreae, M. O.; Gelencser, A., Black carbon or brown carbon? The nature of light-absorbing carbonaceous aerosols. *Atmos. Chem. Phys.* **2006,** *6*, 3131-3148.
16. Tuccella, P.; Curci, G.; Pitari, G.; Lee, S.; Jo, D. S., Direct radiative effect of absorbing aerosols: sensitivity to mixing state, brown carbon and soil dust refractive index and shape. *Journal of Geophysical Research: Atmospheres* **2020,** *125*, (2), e2019JD030967. doi:10.1029/2019JD030967
17. Laskin, A.; Laskin, J.; Nizkorodov, S. A., Chemistry of Atmospheric Brown Carbon. *Chem. Rev.* **2015,** *115*, 4335-4382. doi:10.1021/cr5006167
18. Lee, H. J.; Aiona, P. K.; Laskin, A.; Laskin, J.; Nizkorodov, S. A., Effect of solar radiation on the optical properties and molecular composition of laboratory proxies of atmospheric brown carbon. *Environ. Sci. Technol.* **2014,** *48*, (17), 10217-10226. doi:10.1021/es502515r
19. Hinks, M. L.; Brady, M. V.; Lignell, H.; Song, M.; Grayson, J. W.; Bertram, A. K.; Lin, P.; Laskin, A.; Laskin, J.; Nizkorodov, S. A., Effect of viscosity on photodegradation rates in complex secondary organic aerosol materials. *Phys. Chem. Chem. Phys.* **2016,** *18*, (13), 8785-8793. doi:10.1039/C5CP05226B
20. Aiona, P. K.; Lee, H. J.; Leslie, R.; Lin, P.; Laskin, A.; Laskin, J.; Nizkorodov, S. A., Photochemistry of Products of the Aqueous Reaction of Methylglyoxal with Ammonium Sulfate. *ACS Earth Space Chem.* **2017,** *1*, (8), 522-532. doi:10.1021/acsearthspacechem.7b00075
21. Aiona, P. K.; Luek, J. L.; Timko, S. A.; Powers, L. C.; Gonsior, M.; Nizkorodov, S. A., Effect of Photolysis on Absorption and Fluorescence Spectra of Light-Absorbing Secondary Organic Aerosols. *ACS Earth Space Chem.* **2018,** *2*, (3), 235-245. doi:10.1021/acsearthspacechem.7b00153
22. Fleming, L. T.; Lin, P.; Roberts, J. M.; Selimovic, V.; Yokelson, R.; Laskin, J.; Laskin, A.; Nizkorodov, S. A., Molecular composition and photochemical lifetimes of brown carbon chromophores in biomass burning organic aerosol. *Atmos. Chem. Phys.* **2020,** *20*, (2), 1105-1129. doi:10.5194/acp-20-1105-2020

23. Dalton, A. B.; Nizkorodov, S. A., Photochemical Degradation of 4-Nitrocatechol and 2,4-Dinitrophenol in a Sugar-Glass Secondary Organic Aerosol Surrogate. *Environ. Sci. Technol.* **2021,** *55*, (21), 14586-14594. doi:10.1021/acs.est.1c04975
24. Fan, X.; Cao, T.; Yu, X.; Wang, Y.; Xiao, X.; Li, F.; Xie, Y.; Ji, W.; Song, J.; Peng, P., The evolutionary behavior of chromophoric brown carbon during ozone aging of fine particles from biomass burning. *Atmos. Chem. Phys.* **2020,** *20*, (8), 4593-4605. doi:10.5194/acp-20-4593-2020
25. Schnitzler, E. G.; Gerrebos, N. G. A.; Carter, T. S.; Huang, Y.; Heald, C. L.; Bertram, A. K.; Abbatt, J. P. D., Rate of atmospheric brown carbon whitening governed by environmental conditions. *Proc. Natl. Acad. Sci. U.S.A.* **2022,** *119*, (38), e2205610119. doi:10.1073/pnas.2205610119
26. Wong, J. P. S.; Nenes, A.; Weber, R. J., Changes in Light Absorptivity of Molecular Weight Separated Brown Carbon Due to Photolytic Aging. *Environ. Sci. Technol.* **2017,** *51*, (15), 8414-8421. doi:10.1021/acs.est.7b01739
27. Zhao, R.; Lee, A. K. Y.; Huang, L.; Li, X.; Yang, F.; Abbatt, J. P. D., Photochemical processing of aqueous atmospheric brown carbon. *Atmos. Chem. Phys.* **2015,** *15*, (11), 6087-6100. doi:10.5194/acp-15-6087-2015
28. Zeng, L.; Dibb, J.; Scheuer, E.; Katich, J. M.; Schwarz, J. P.; Bourgeois, I.; Peischl, J.; Ryerson, T.; Warneke, C.; Perring, A. E.; Diskin, G. S.; DiGangi, J. P.; Nowak, J. B.; Moore, R. H.; Wiggins, E. B.; Pagonis, D.; Guo, H.; Campuzano-Jost, P.; Jimenez, J. L.; Xu, L.; Weber, R. J., Characteristics and evolution of brown carbon in western United States wildfires. *Atmos. Chem. Phys.* **2022,** *22*, (12), 8009-8036. doi:10.5194/acp-22-8009-2022
29. Zhong, M.; Jang, M., Dynamic light absorption of biomass-burning organic carbon photochemically aged under natural sunlight. *Atmos. Chem. Phys.* **2014,** *14*, (3), 1517-1525, 9 pp. doi:10.5194/acp-14-1517-2014
30. Forrister, H.; Liu, J.; Scheuer, E.; Dibb, J.; Ziemba, L.; Thornhill, K. L.; Anderson, B.; Diskin, G.; Perring, A. E.; Schwarz, J. P.; Campuzano-Jost, P.; Day, D. A.; Palm, B. B.; Jimenez, J. L.; Nenes, A.; Weber, R. J., Evolution of brown carbon in wildfire plumes. *Geophys. Res. Lett.* **2015,** *42*, (11), 4623-4630. doi:10.1002/2015GL063897
31. Hems, R. F.; Abbatt, J. P. D., Aqueous Phase Photo-oxidation of Brown Carbon Nitrophenols: Reaction Kinetics, Mechanism, and Evolution of Light Absorption. *ACS Earth Space Chem.* **2018,** *2*, (3), 225-234. doi:10.1021/acsearthspacechem.7b00123
32. De Haan, D. O.; Hawkins, L. N.; Welsh, H. G.; Pednekar, R.; Casar, J. R.; Pennington, E. A.; de Loera, A.; Jimenez, N. G.; Symons, M. A.; Zauscher, M.; Pajunoja, A.; Caponi, L.; Cazaunau, M.; Formenti, P.; Gratien, A.; Pangui, E.; Doussin, J. F., Brown carbon production in ammonium- or amine-containing aerosol particles by reactive uptake of methylglyoxal and photolytic cloud cycling. *Environ. Sci. Technol.* **2017,** *51*, (13), 7458-7466. doi:10.1021/acs.est.7b00159
33. Jimenez, N. G.; Sharp, K. D.; Gramyk, T.; Ugland, D. Z.; Tran, M.-K.; Rojas, A.; Rafla, M. A.; Stewart, D.; Galloway, M. M.; Lin, P.; Laskin, A.; Cazaunau, M.; Pangui, E.; Doussin, J.-F.; De Haan, D. O., Radical-Initiated Brown Carbon Formation in Sunlit Carbonyl–Amine–Ammonium Sulfate Mixtures and Aqueous Aerosol Particles. *ACS Earth Space Chem.* **2022,** *6*, 228. doi:10.1021/acsearthspacechem.1c00395
34. Schnitzler, E. G.; Liu, T.; Hems, R.; Abbatt, J., Emerging investigator series: Heterogeneous OH oxidation of primary brown carbon aerosol: effects of relative humidity and volatility. *Environ. Sci.: Process. Impacts* **2020**. doi:10.1039/D0EM00311E

35. Sharp, J. R.; Grace, D. N.; Ma, S.; Woo, J. L.; Galloway, M. M., Competing Photochemical Effects in Aqueous Carbonyl/Ammonium Brown Carbon Systems. *ACS Earth Space Chem.* **2021**. doi:10.1021/acsearthspacechem.1c00165
36. Pye, H. O. T.; Nenes, A.; Alexander, B.; Ault, A. P.; Barth, M. C.; Clegg, S. L.; Collett Jr, J. L.; Fahey, K. M.; Hennigan, C. J.; Herrmann, H.; Kanakidou, M.; Kelly, J. T.; Ku, I. T.; McNeill, V. F.; Riemer, N.; Schaefer, T.; Shi, G.; Tilgner, A.; Walker, J. T.; Wang, T.; Weber, R.; Xing, J.; Zaveri, R. A.; Zuend, A., The acidity of atmospheric particles and clouds. *Atmos. Chem. Phys.* **2020,** *20*, (8), 4809-4888. doi:10.5194/acp-20-4809-2020
37. Volkamer, R.; Ziemann, P. J.; Molina, M. J., Secondary organic aerosol formation from acetylene (C_2H_2): seed effect on SOA yields due to organic photochemistry in the aerosol aqueous phase. *Atmos. Chem. Phys.* **2009,** *9*, 1907-1928. doi:10.5194/acp-9-1907-2009
38. Eurochamp, Eurochamp-2: Integration of European Simulation Chambers for Investigating Atmospheric Processes. In CEAM: Valencia, Spain, 2010. https://data.eurochamp.org/data-access/ir-spectra/
39. De Haan, D. O.; Tapavicza, E.; Riva, M.; Cui, T.; Surratt, J.; Smith, A. C.; Jordan, M.-C.; Nilakantan, S.; Almodovar, M.; Stewart, T. N.; de Loera, A.; De Haan, A. C.; Cazaunau, M.; Gratien, A.; Pangui, E.; Doussin, J. F., Nitrogen-containing, light-absorbing oligomers produced in aerosol particles exposed to methylglyoxal, photolysis, and cloud cycling. *Environ. Sci. Technol.* **2018,** *52*, (7), 4061-4071. doi:10.1021/acs.est.7b06105
40. Brandt, C.; van Eldik, R., Transition Metal-Catalyzed Oxidation of Sulfur(IV) Oxides. Atmospheric-Relevant Processes and Mechanisms. *Chem. Rev.* **1995,** *95*, (1), 119-190. doi:10.1021/cr00033a006
41. Coddens, E. M.; Huang, L.; Wong, C.; Grassian, V. H., Influence of Glyoxal on the Catalytic Oxidation of S(IV) in Acidic Aqueous Media. *ACS Earth Space Chem.* **2019,** *3*, (1), 142-149. doi:10.1021/acsearthspacechem.8b00168
42. Kwong, K. C.; Chim, M. M.; Davies, J. F.; Wilson, K. R.; Chan, M. N., Importance of sulfate radical anion formation and chemistry in heterogeneous OH oxidation of sodium methyl sulfate, the smallest organosulfate. *Atmos. Chem. Phys.* **2018,** *18*, (4), 2809-2820. doi:10.5194/acp-18-2809-2018
43. Huang, L.; Liu, T.; Grassian, V. H., Radical-Initiated Formation of Aromatic Organosulfates and Sulfonates in the Aqueous Phase. *Environ. Sci. Technol.* **2020,** *54*, (19), 11857-11864. doi:10.1021/acs.est.0c05644
44. Surratt, J. D.; Kroll, J. H.; Kleindienst, T. E.; Edney, E. O.; Claeys, M.; Sorooshian, A.; Ng, N. L.; Offenberg, J. H.; Lewandowski, M.; Jaoui, M.; Flagan, R. C.; Seinfeld, J. H., Evidence for organosulfates in secondary organic aerosol. *Environ. Sci. Technol.* **2007,** *41*, (2), 517-527. doi:10.1021/es062081q
45. Walser, M. L.; Desyaterik, Y.; Laskin, J.; Laskin, A.; Nizkorodov, S. A., High-resolution mass spectrometric analysis of secondary organic aerosol produced by ozonation of limonene. *Phys. Chem. Chem. Phys.* **2008,** *10*, (7), 1009-1022. doi:10.1039/B712620D
46. Alpert, P. A.; Dou, J.; Corral Arroyo, P.; Schneider, F.; Xto, J.; Luo, B.; Peter, T.; Huthwelker, T.; Borca, C. N.; Henzler, K. D.; Schaefer, T.; Herrmann, H.; Raabe, J.; Watts, B.; Krieger, U. K.; Ammann, M., Photolytic radical persistence due to anoxia in viscous aerosol particles. *Nat. Commun.* **2021,** *12*, (1), 1769. doi:10.1038/s41467-021-21913-x
47. Peters, J.-H.; Dette, H. P.; Koop, T., Glyoxal as a Potential Source of Highly Viscous Aerosol Particles. *ACS Earth Space Chem.* **2021,** *5*, (12), 3324-3337. doi:10.1021/acsearthspacechem.1c00245

48. Graber, E. R.; Rudich, Y., Atmospheric HULIS: How humic-like are they? A comprehensive and critical review. *Atmos. Chem. Phys.* **2006,** *6*, 729-753.
49. Bones, D. L.; Henricksen, D. K.; Mang, S. A.; Gonsior, M.; Bateman, A. P.; Nguyen, T. B.; Cooper, W. J.; Nizkorodov, S. A., Appearance of strong absorbers and fluorophores in limonene-O_3 secondary organic aerosol due to NH_4^+-mediated chemical aging over long time scales. *J. Geophys. Res. Atmos.* **2010,** *115*, (D5), D05203/1-14. doi:10.1029/2009JD012864
50. Olson, T. M.; Hoffmann, M. R., Formation kinetics, mechanism, and thermodynamics of glyoxylic acid-sulfur(IV) adducts. *J. Phys. Chem.* **1988,** *92*, (14), 4246-4253. doi:10.1021/j100325a050
51. Betterton, E. A.; Hoffmann, M. R., Kinetics, mechanism, and thermodynamics of the reversible reaction of methylglyoxal (CH3COCHO) with S(IV). *J. Phys. Chem. A* **1987,** *91*, (11), 3011-3020. doi:10.1021/j100295a074
52. Hawkins, L. N.; Baril, M. J.; Sedehi, N.; Galloway, M. M.; De Haan, D. O.; Schill, G. P.; Tolbert, M. A., Formation of semi-solid, oligomerized aqueous SOA: Lab simulations of cloud processing. *Environ. Sci. Technol.* **2014,** *48*, (4), 2273-2280. doi:10.1021/es4049626
53. Altemose, B.; Gong, J.; Zhu, T.; Hu, M.; Zhang, L.; Cheng, H.; Zhang, L.; Tong, J.; Kipen, H. M.; Strickland, P. O.; Meng, Q.; Robson, M. G.; Zhang, J., Aldehydes in Relation to Air Pollution Sources: A Case Study around the Beijing Olympics. *Atmos. Environ.* **2015,** *109*, 61-69. doi:10.1016/j.atmosenv.2015.02.056
54. Xue, L.; Ding, A.; Gao, J.; Wang, T.; Wang, W.; Wang, X.; Lei, H.; Jin, D.; Qi, Y., Aircraft measurements of the vertical distribution of sulfur dioxide and aerosol scattering coefficient in China. *Atmos. Environ.* **2010,** *44*, (2), 278-282. doi:https://doi.org/10.1016/j.atmosenv.2009.10.026
55. Shiraiwa, M.; Li, Y.; Tsimpidi, A. P.; Karydis, V. A.; Berkemeier, T.; Pandis, S. N.; Lelieveld, J.; Koop, T.; Pöschl, U., Global distribution of particle phase state in atmospheric secondary organic aerosols. *Nat. Commun.* **2017,** *8*, (1), 15002. doi:10.1038/ncomms15002
56. Pani, S. K.; Lin, N.-H.; Griffith, S. M.; Chantara, S.; Lee, C.-T.; Thepnuan, D.; Tsai, Y. I., Brown carbon light absorption over an urban environment in northern peninsular Southeast Asia. *Environ. Pollut.* **2021,** *276*, 116735. doi:https://doi.org/10.1016/j.envpol.2021.116735
57. Deng, J.; Ma, H.; Wang, X.; Zhong, S.; Zhang, Z.; Zhu, J.; Fan, Y.; Hu, W.; Wu, L.; Li, X.; Ren, L.; Pavuluri, C. M.; Pan, X.; Sun, Y.; Wang, Z.; Kawamura, K.; Fu, P., Measurement report: Optical properties and sources of water-soluble brown carbon in Tianjin, North China – insights from organic molecular compositions. *Atmos. Chem. Phys.* **2022,** *22*, (10), 6449-6470. doi:10.5194/acp-22-6449-2022
58. Rathod, T.; Sahu, S. K.; Tiwari, M.; Yousaf, A.; Bhangare, R. C.; Pandit, G. G., Light Absorbing Properties of Brown Carbon Generated from Pyrolytic Combustion of Household Biofuels. *Aerosol Air Qual. Res.* **2017,** *17*, (1), 108-116. doi:10.4209/aaqr.2015.11.0639
59. Zhang, Y.; Albinet, A.; Petit, J.-E.; Jacob, V.; Chevrier, F.; Gille, G.; Pontet, S.; Chrétien, E.; Dominik-Sègue, M.; Levigoureux, G.; Močnik, G.; Gros, V.; Jaffrezo, J.-L.; Favez, O., Substantial brown carbon emissions from wintertime residential wood burning over

France. *Sci. Total Environ.* **2020,** *743,* 140752.
doi:https://doi.org/10.1016/j.scitotenv.2020.140752

TOC artwork

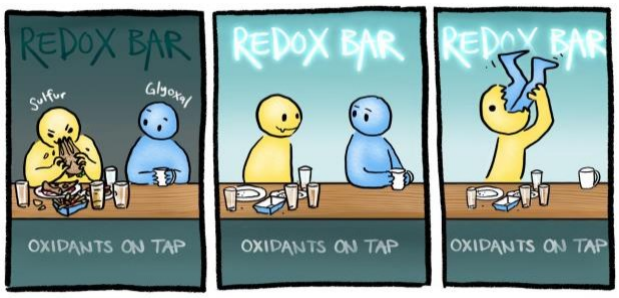
REDOX BAR
Sulfur
Glyoxal
OXIDANTS ON TAP
REDOX BAR
OXIDANTS ON TAP
REDOX BAR
OXIDANTS ON TAP